Piezoelectric performance of PZT-based materials with aligned porosity: experiment and modelling

To cite this article before publication: Yan Zhang *et al* 2019 *Smart Mater. Struct.* in press https://doi.org/10.1088/1361-665X/ab5018

Piezoelectric performance of PZT-based materials with aligned porosity: experiment and modelling

Yan Zhang[1], Vitaly Yu Topolov[2,3], Ashura N Isaeva[2], Christopher R Bowen[1], Holly Pearce[1], Hamideh Khanbareh[1]

[1]Department of Mechanical Engineering, University of Bath, Bath BA2 7AY, UK

[2]Department of Physics, Southern Federal University, 344090 Rostov-on-Don, Russia

[3]Institute of High Technologies and Piezotechnics, Southern Federal University, 344090 Rostov-on-Don, Russia

E-Mail: vutopolov@sfedu.ru

Received March 2019, revised August 2019

Abstract. A new micromechanical model is proposed to analyse the piezoelectric properties of freeze-cast porous composite materials based on a ferroelectric lead zirconate titanate-type (PZT) ceramics. The important influence of the composite microgeometry and the porous ceramic matrix on the piezoelectric coefficients d_{3j}^* and g_{3j}^* and the piezoelectric anisotropy factor $d_{33}^*/|d_{31}^*|$ in the porosity range of m_p = 0.2–0.6 is evaluated and discussed. The resulting piezoelectric parameters of parallel-connected freeze-cast composites with highly aligned pore channels are then compared to those of PZT-based porous materials with randomly distributed porosity. Due to the relatively large piezoelectric coefficients $d_{33}^* \sim 10^2$ pC N^{-1},

$g_{33}^{*} \approx$ 40–100 mV m N^{-1}, anisotropy factor $d_{33}^{*} / |d_{31}^{*}| \approx$ 3–5 and the presence of aligned porous channels, the parallel-connected freeze-cast composite has advantages over conventional monolithic PZT-type ceramics (e.g. g_{33} = 24.2 mV m N^{-1} and $d_{33}/|d_{31}| = 2.2$ in the PZT-5 ceramic) and is suitable for piezoelectric transducer, sensor, acoustic, and energy-harvesting applications.

Keywords: piezoelectric coefficients, piezoelectric anisotropy, porous medium, freeze-cast porous composite

Introduction

It has been reported that porous piezoelectric materials, in both ceramic and composite forms, exhibit electromechanical properties that strongly depend on the ceramic volume fraction and microgeometry of pores [1–3], processing method [4–7] and poling conditions [8, 9]. The relationships in the well-known fundamental triangle of 'composition – structure – properties' [10] for porous ferroelectric ceramics (FCs) are intricate and complex for a number of reasons. Firstly, the 'composition' of the porous material depends not only on the chemical composition of the FC component (with possible composition fluctuations therein, especially near the morphotropic phase boundary [11]), but also on the volume fraction of pores within the porous sample, m_p. Secondly, the 'structure' relates to features of the pore structure, the microstructure of the FC and the specific connectivity patterns in the composite. Thirdly, the physical 'properties' of the porous material are regarded as *effective* [1–3, 5, 7], and are averaged by taking into account the microgeometry, the properties of the FC, the porosity fraction, and degree of poling.

In recent years, novel piezo-active porous composites based on lead zirconate titanate (PZT) FCs have been manufactured by means of the freeze-casting method, and the characteristics of these novel materials have been typically studied in a porosity m_p range of 0 to 60 vol. %, as reported in work [12–16]. Much effort have been made to form so-called one-dimensional porous structures that are described as 3–1- or 1–3-type [12–14] in terms of the composite connectivity

patterns in terms of work [3, 17]. Undoubtedly, of an independent interest is the control over FC grain orientations and domain configurations within individual grains of the manufactured porous samples [13] and a control over the pore size and other microgeometric characteristics of the materials [14]. Moreover, the freeze-casting method has been employed to create 3–1 PZT FC / epoxy composites [18]. Despite the vast experimental data on the aforementioned materials with the one-dimensional porous structures [12–14, 18], their piezoelectric anisotropy factor d_{33}^*/d_{31}^* has yet to be analysed, even in a restricted porosity range. To provide further progress in the field of porous piezoelectric materials and improve their properties, there is a need for a detailed understanding of the relationships in the aforementioned fundamental triangle of composition, structure and properties.

This paper provides a detailed analysis of the piezoelectric properties and their anisotropy factors in a freeze-cast PZT-based material with aligned porosity, and introduces a model to understand the piezoelectric properties, their anisotropy and related parameters of this material at porosity m_p = 0.2–0.6. The potential benefits of forming aligned porosity, as opposed to randomly distributed porosity, are also quantified. A need for a new micromechanical model of the freeze-cast composite material is motivated by the complex relations between the microgeometry and properties in piezo-active composites [3] and from a strong dependence of their piezoelectric response on porosity [1, 2, 4].

Experimental

The method to manufacture the piezoelectric freeze-cast PZT-based material is described in our previous work [15, 16]. The ferroelectric component used for the manufacture of the porous FC is a commercial lead zirconate titanate powder (PZT-51, Zibo Yuhai Electronic Ceramic Co., Ltd, Zibo, China). During the freeze-casting process, dense columns and cellular channels are formed in samples at the beginning of the freezing cycle; such a structure is formed since the formation of ice crystals lead to the ceramic particles being forced into dense columns, while the cellular and more porous channels represent the locations of the ice crystals which are removed by freeze drying, as shown in figure 1. After the removal of the dense and cellular layers formed at the initial phase of the freeze casting process, typically <2 mm thickness, a homogenous lamellar structure was formed and was utilised for the following characterisation study. The freeze-cast and freeze-dried porous samples were then sintered to form porous materials with the FC aligned in the freezing direction, which can then be cut either perpendicular or parallel to the freezing direction. The two main composite structures formed can be considered as either parallel-connected (when cut perpendicular to freezing direction) and series-connected (when cut parallel to freezing direction). The parallel-connected system with the PZT columns aligned on the poling direction will be the focus of our present paper. The system of the parallel-connected PZT columns in the sample facilitates its poling in the electric field $\boldsymbol{E}$ oriented along these columns, see the vertical direction in figure 1. The thickness of the samples

for characterisation is ca. 1.0 mm. For comparison, porous PZT with randomly distributed pores were fabricated by the burned out polymer spheres (BURPS) process [3, 5]. PZT powders were mixed with ethanol and pore forming agent-polyethylene glycol (PEG) at mass fractions based on the PZT powders. The obtained mixture powders were uni-axially pressed to form pellets of 13 mm in diameter and 1.5 mm in thickness.

The resulting microstructures of the manufactured samples, their pore morphology and the structure of the PZT walls were studied by scanning electron microscopy (SEM, JSM-6480LV, JEOL Techniques, Tokyo, Japan). The porosity of the samples (m_p) was determined by the Archimedes method [19]. Corona poling was conducted on the samples at temperature T = 393 K by applying a potential difference of 14 kV to a point source above the sample for 15 min and the cooled to T = 303 K under a corona field, and the poled samples are relaxed for 24 h before measurements of their piezoelectric and dielectric properties. Following notations [3], in the present paper we will use the asterisk (*) to denote the effective (or averaged) physical properties of the poled freeze-cast porous composite material.

The longitudinal piezoelectric strain coefficient d_{33}^* and the transverse piezoelectric strain coefficient d_{31}^* were measured using a Berlincourt Piezometer (PM25, Take Control, UK). Measurements of the relative dielectric permittivity $\varepsilon_{33}^{*\sigma} / \varepsilon_0$ at a constant mechanical were carried out at frequencies of f = 1 Hz – 1 MHz at room temperature using an impedance analyzer (Solartron 1260,

Hampshire, UK). The properties of poled monolithic PZT-51 FC at room temperature are characterised by the piezoelectric coefficients $d_{33}^{(FC)}$ = 552 pC N^{-1} and $d_{31}^{(FC)}$ = –182 pC N^{-1} and relative dielectric permittivity $\varepsilon_{33}^{(FC),\sigma}$ / ε_0 = 2158 (at f = 1 kHz). To the best of our knowledge, the full set of electromechanical constants is yet to be measured on poled monolithic PZT-51 FC samples.

SEM images of microstructures of parallel-connected samples in the direction, that is parallel to the unidirectional freezing direction, are shown in figure 2(a)–(d). Highly aligned and homogeneous lamellar pore channels with a pore width of 15–25 μm and a dense FC-wall thickness of 5–15 μm are achieved in the manufactured samples; we define the volume fraction of these FC-walls as m and the volume fraction of air in the porous channels as μ_p. In contrast to porous FC structures with uniformly distributed porosity [20], a large fraction of the FC links in the pore volume of the freeze-cast porous samples determines their improved piezoelectric properties when there is a parallel connection of layers. The FC links can also improve poling of the sample and its resulting piezoelectric performance. It should be added that the character of the distribution of the porosity and pore size (10 – 30 μm) in the manufactured samples, and the related modelling features are to be considered as a subject of a future independent study.

The pore volume-fraction (m_p) dependences of normalised parameters X^* / $X^{(FC)}$ and piezoelectric anisotropy factor d_{33}^*/d_{31}^* of the poled parallel-connected samples are shown in figure 2(e). The piezoelectric coefficient g_{33}^*, that

characterises the piezoelectric sensitivity along the poling axis OX_3, is determined from measurements of the piezoelectric coefficient d_{33}^* and dielectric permittivity $\varepsilon_{33}^{*\sigma}$, and the aforementioned parameters are linked as follows:

$$g_{33}^* = d_{33}^* / \varepsilon_{33}^{*\sigma}. \quad (1)$$

The energy harvesting figure of merit

$$(Q_{33}^*)^2 = d_{33}^* g_{33}^* = (d_{33}^*)^2 / \varepsilon_{33}^{*\sigma} \quad (2)$$

is used to characterise the 'signal – noise' ratio [3] in the poling direction. The normalised parameters with respect to the monolithic FC $X^* / X^{(FC)}$ ($X = d_{ij}$, g_{ij} etc.) is of value for the assessment [3, 4, 7] of the performance of porous materials based on FCs.

Curves 1 and 2 in figure 2(e) indicate a weakening of the piezoelectric effect due to the presence of porosity in the structure, and its influence is stronger at larger levels of porosity m_p values and in the lateral direction (OX_1 direction). This influence is inseparably connected with the piezoelectric anisotropy due to the porous structure and other microgeometric factors, see figure 2(a–d). The d_{33}^* and $|d_{31}^*|$ decrease trends [see curves 1 and 2 in figure 2(e)] are combined to provide a g_{33}^* increase trend [see curve 3 in figure 2(e)], and this increase is important for potential sensor applications. It should be noted that in the real freeze-cast parallel-connected sample, no difference between the piezoelectric coefficients d_{31}^* and d_{32}^* is observed due to the mosaic, non-unidirectional character of the arrangement of

the FC-walls [see figure 2(d)] as a result of the growth of multiple ice crystals in the sample.

The inequality

$$d_{33}^{*} \,/\, d_{33}^{(FC)} > d_{31}^{*} \,/\, d_{31}^{(FC)} \tag{3}$$

holds in the wide m_p range, cf. curves 1 and 2 in figure 2(e) and condition (3) influences the anisotropy factor d_{33}^{*}/d_{31}^{*} [curve 5 in figure 2(e)]. The increase in both g_{33}^{*} and $(Q_{33}^{*})^2$, which has been determined from equations (1) and (2), with porosity level are a consequence of the monotonic decrease of $\varepsilon_{33}^{*\sigma}$, which is more appreciable than the decrease of d_{33}^{*} in the same m_p range. This effect leads to a monotonic increase of $g_{33}^{*} \,/\, g_{33}^{(FC)}$ and $(Q_{33}^{*})^2 \,/\, (Q_{33}^{(FC)})^2$ with increasing level of porosity, see curves 3 and 4 in figure 2(e).

It should be added that the thermal stability of the studied piezoelectric properties is related to the relatively high Curie point of the FC component (T_C = 473 K) and undergoes minor changes at the transition from the parallel-connected to series-connected composite structure. Normally, the operating temperature of a piezoelectric ceramics is below one half of the Curie temperature (in °C) [21]. The PZT powder used in this work is similar to the PZT 5H FC, with small changes in the coupling coefficient, dielectric loss and permittivity below its half point of Curie temperature of 100 °C [22].

As a comparison to the freeze-cast material micrographs in figure 2(a)–(d), in figure 3 we show SEM images of the microstructures, normalised parameters X^{*} /

$X^{(FC)}$ and piezoelectric anisotropy factor d_{33}^{*}/d_{31}^{*} of composites with randomly distributed pores, where $X^{(FC)}$ is the property of the poled FC component. Porous PZT with the equi-axed spherical pores, due to the uniform shape and distribution of the pore former (i.e., PEG in our experiments), can be seen in figure 3(a) and (b). As more PEG being added, higher levels of porosity and larger pore sizes can be obtained, as shown in figure 3(b). The graphs in figure 3(c) and (d) suggest that the piezoelectric properties related to the piezoelectric coefficients d_{3j}^{*} and their anisotropy become less favourable and fall more quickly with porosity level in comparison to the parameters of the material with the freeze-cast parallel-connected layers, see figure 2(e). The higher piezoelectric activity (or larger $d_{3j}^{*}/d_{3j}^{(FC)}$ ratios) and the larger anisotropy of d_{3j}^{*} in the parallel-connected porous samples [see curves 1, 2 and 5 in figure 2(e)] make this freeze-cast material more promising in sensor, and transducer applications.

Model of the composite and its effective properties

The piezoelectric properties and related parameters of the parallel-connected freeze-cast porous material are now analysed using a model based on a 'composite in composite', as pictured in figure 4 which shows the model different orientations. It is assumed that monolithic FC rods are surrounded by a porous FC matrix and is regularly distributed over the sample, figure 4(a). The FC rods represent the dense columns as shown in figure 4(a), while the porous matrix represents the porous channels that surround these rods. The porous FC matrix acts as a continuous

medium with a system of aligned isolated pores which is characterised by 3–0 connectivity. The monolithic FC rods are parallel to the OX_3 axis, which is the poling axis for composite as a whole. The elliptical cross section of each rod by the (X_1OX_2) plane [see figure 4(a) and (c)] is described by the equation

$$(x_1 / a_1)^2 + (x_2 / a_2)^2 = 1 \quad (4)$$

in the rectangular co-ordinate system $(X_1X_2X_3)$. In equation (4), a_1 and a_2 are semi-axes of the elliptical cross section, see figure 4(c). The aspect ratio of the elliptical cross section is defined as $\eta = a_1 / a_2$ and we assume that the centres of symmetry of the rod bases are located at apices of rectangles that form a simple lattice in the (X_1OX_2) plane.

Within the porous matrix, the air pores are characterised by its semi-axes a_{p1}, $a_{p2} = a_{p1}$, and a_{p3}, where the aspect ratio is defined as $\rho_p = a_{p1}/a_{p3}$. The spheroidal shape of the air pore is described by the equation

$$(x_1 / a_{p1})^2 + (x_2 / a_{p1})^2 + (x_3 / a_{p3})^2 = 1 \quad (5)$$

in the co-ordinate system $(X_1X_2X_3)$. The pores are considered to be regularly distributed in the FC medium that surrounds the monolithic FC rods in the composite, as shown in figure 3, and centres of symmetry of the air pores are also located in apices of rectangular parallelepipeds which form a simple lattice.

Taking into account the presence of the air pores in the matrix and the volume fraction of the monolithic FC rods m in the composite (figure 4), we describe the total porosity of the composite as $m_p = (1-m)\mu_p$, where μ_p is the volume fraction of the pores in the matrix that surrounds the rods.

The composite shown in figure 4 is characterised by 1–3–0 connectivity, and in the limiting case, at $\eta = 0$ or $\eta \to \infty$, the connectivity indexes would be 2–2–0. A 2–2–0 composite in this case represents a system of monolithic and porous FC layers that are parallel-connected, as in figure 2. The effective piezoelectric, dielectric and elastic (i.e., electromechanical) properties of the 1–3–0 composite shown in figure 4(a) are predicted on the assumption that the linear sizes of each pore [see the semi-axes in equation (5)] are much smaller than the diameter of each monolithic FC rod.

In the first stage, the effective properties of the 3–0 porous medium are determined within the framework of Eshelby's concept [2, 3, 23] based on spheroidal inclusions in a heterogeneous solid (dilute approximation) which is expressed by a 9×9 matrix

$$|| C^{(pm)} || = || C^{(FC)} ||\cdot[|| I || - \mu_p(|| I || - (1 - \mu_p)|| S^{(FC)} ||)^{-1}]. \quad (6)$$

In equation (6),

$$|| C^{(FC)} || = \begin{pmatrix} ||c^{(FC),E}|| & ||e^{(FC)}||^t \\ ||e^{(FC)}|| & -||\varepsilon^{(FC),\xi}|| \end{pmatrix} \quad (7)$$

is a 9×9 matrix that characterises the electromechanical properties of the poled FC, $|| I ||$ is a 9×9 identity matrix, and $|| S^{(FC)} ||$ is a 9×9 matrix that contains the Eshelby tensor components depending on elements of $|| C^{(FC)} ||$ and the aspect ratio ρ_p of the pores. In equation (7), $|| c^{(FC),E} ||$ is a 6×6 matrix of the elastic moduli of the FC at E = const, $|| e^{(FC)} ||$ is a 3×6 matrix of the piezoelectric coefficients of the

FC, $\| \varepsilon^{(FC),\xi} \|$ is a 3 × 3 matrix of the dielectric permittivities of the FC at ξ = const, and the superscript *t* denotes the transposition.

In the second stage, the effective properties of the 1–3 system of 'monolithic FC rods – porous FC matrix' are evaluated using the effective field method [3]. This method enables us to take into account the electromechanical interaction between the FC rods in the porous matrix that is assumed to be either non-poled (isotropic) or poled along the OX_3 axis (transversely isotropic). The effective properties of the composite are given by a 9 × 9 matrix as follows:

$$\| C^* \| = \| C^{(pm)} \| + m(\| C^{(FC)} \| - \| C^{(pm)} \|)[\| I \| + (1-m)\| S \| \| C^{(pm)} \|^{-1}(\| C^{(FC)} \| - \| C^{(pm)} \|)]^{-1}. \quad (8)$$

The $\| C^{(pm)} \|$ and $\| C^* \|$ matrices from equations (6) and (8), respectively, have the structure shown for $\| C^{(FC)} \|$ in equation (7). The $\| S \|$ matrix from equation (8) contains the Eshelby tensor components that are related to the circular cylinder [i.e., the base of the monolithic FC rod, see figure 4(a)] and depend on the properties of the porous FC medium that surrounds the rods. The $\| C^* \|$ matrix from equation (8) can be represented in the general form as $\| C^* \| = \| C^*(m, \eta, \mu_p, \rho_p) \|$. The $\| C^* \|$ matrix from equation (8) is determined in the longwave approximation, which assumes that the wavelength of any external field is much greater than the diameter of each monolithic FC rod in the composite in figure 3.

Taking into account the elements of $\| C^* \|$ from equation (8) and formulae for the piezoelectric medium [24], we evaluate the piezoelectric coefficients d_{3j}^* and g_{3j}^* (j = 1, 2 and 3), anisotropy factors

$$\zeta_{d1}^{*} = d_{33}^{*} / d_{31}^{*} = g_{33}^{*} / g_{31}^{*} \text{ and } \zeta_{d2}^{*} = d_{33}^{*} / d_{32}^{*} = g_{33}^{*} / g_{32}^{*}, \quad (9)$$

and energy harvesting figure of merit $(Q_{33}^{*})^2$ from equation (2). To evaluate the normalised parameters $X^* / X^{(FC)}$, we use constants of the perovskite-type FCs such as PZT-5 and PCR-7M; see data in table 1. This is undertaken due to the lack of the full set of electromechanical constants of the PZT-51 FC that is used to manufacture the freeze-cast samples. As a result of the ∞mm symmetry [11, 24, 25] of the FC component that is poled along the OX_3 axis, the equalities $d_{31}^{(FC)} = d_{32}^{(FC)}$ and $g_{31}^{(FC)} = g_{32}^{(FC)}$ hold.

It should be added that the model put forward (figure 4) to interpret the piezoelectric performance and related parameters of the freeze-cast porous material strongly differs from the model by Roscow et al. [26]. In work [26], finite element modeling is applied to characterise the performance of freeze-cast porous $BaTiO_3$ by taking into account features of the distribution of pores, poled and unpoled FC regions, and complex porous regions. The model [26] is used to interpret the longitudinal piezoelectric and dielectric responses of the freeze-cast porous $BaTiO_3$ samples. By applying the model shown in figure 4, we are able to place an emphasis on the 'microgeometry – properties' relations in the presence of FC regions with variable porosity. Here we also show an influence of the porous structure on the piezoelectric anisotropy that was not considered in work [26].

Comparison of results and discussion

We now examine the calculated normalised parameters $X^* / X^{(FC)}$ and anisotropy factors ζ_{d1}^* and ζ_{d2}^* predicted from the model, where we assume that the porous FC matrix of the composite, shown in figure 4, is either non-poled (figure 5) or poled along the OX_3 axis (figure 6). For this data we assume a constant FC rod aspect ratio of $\eta = 0.1$, so that the FC rods in the (X_1OX_2) plane [see figure 4(c)] have an almost rectangular form, and a system of such rods that are distributed regularly over the sample is analogous to a laminar structure of the 2–2-type parallel-connected composite in figure 2 [3].

Changes in μ_p and ρ_p enable us to vary the elastic properties and their anisotropy in the porous matrix. This leads to changes in the piezoelectric performance and related parameters of the composite, and graphs in figures 5 and 6 illustrate these changes. With regard to the aspect ratio of the ferroelectric rods of $\eta = 0.1$, this is close to that of the monolithic FC regions shown in figure 2(d). The aspect ratio of the pore $\mu_p = 10$ represents highly oblate pores, whose shape strongly influences the elastic anisotropy of the porous matrix and the size of the pores are small in comparison to ferroelectric rods. A large total porosity $m_p = 0.5$ or 0.7 is selected to represent the porous matrix of the porous channels, and increasing m_p results in an increase in the specific volume of the pores in the porous channels, which can be either poled or non-poled.

Graphs in figures 5 and 6 suggest that agreement between the calculated and experimental parameters is achieved on various levels of porosity of the sample m_p with a relatively large porosity of the matrix μ_p= 0.5–0.7. At relatively low total

porosity levels of $m_p < 0.4$, the presence of a poled porous FC matrix can influence the piezoelectric response of the sample more actively. It should be noted that the average of the anisotropy factors ζ_{d1}^{*} and ζ_{d2}^{*} [see equations (9) and figure 5(f) and (g)] is consistent with the experimental d_{33}^{*}/d_{31}^{*} value in the whole range of m_p.

The calculated values of g_{33}^{*} / $g_{33}^{(FC)}$ and $(Q_{33}^{*})^2$ / $(Q_{33}^{(FC)})^2$ from the model are larger than the experimental parameters; see, for instance, data in figures 5(d) and (e) and 6(d). The larger predicted g_{33}^{*} / $g_{33}^{(FC)}$ and $(Q_{33}^{*})^2$ / $(Q_{33}^{(FC)})^2$ values are observed in the presence of both poled and non-poled porous FC matrices and may be due to the assumption of a system of ideally aligned air pores at ρ_p = const in the model shown in figure 4. A system of highly oblate pores with an aspect ratio $\rho_p >> 1$ promotes an elastic anisotropy that influences the anisotropy factors ζ_{d1}^{*} and ζ_{d2}^{*} from equations (9) and leads to a smaller dielectric permittivity $\varepsilon_{33}^{*\sigma}$ of the composite. This is achieved due to a decrease of the dielectric response along the OX_3 axis in a medium where the system of the layer-like pores violates a continuous distribution of the FC component along the same axis. The smaller $\varepsilon_{33}^{*\sigma}$ value then leads to larger g_{33}^{*} / $g_{33}^{(FC)}$ and $(Q_{33}^{*})^2$ / $(Q_{33}^{(FC)})^2$ values in accordance with equations (1) and (2). We add that the similar decrease of $\varepsilon_{33}^{*\sigma}$ influences both g_{33}^{*} and $(Q_{33}^{*})^2$ of the parallel-connected 2–2 and 1–3 FC-based composites wherein the poled FC component is distributed continuously along the poling axis OX_3 [3].

Changes in the aspect ratio of the FC rod base η do not lead to drastic changes in the piezoelectric coefficients d_{3j}^{*} (j = 1 and 2), see figure 7. In the range of $0 \leq \eta \leq 1$, the piezoelectric coefficient d_{33}^{*} undergoes changes of less than 1% irrespective of characteristics of the porous FC matrix. This is a result of the continuous distribution of the poled FC rods along the poling axis OX_3. On approaching the condition $\eta \to 1$ and equi-axed rods results in $d_{32}^{*} \to d_{31}^{*}$ and $g_{32}^{*} \to g_{31}^{*}$ and any distinction between the piezoelectric responses along the OX_2 and OX_1 axes disappears. The difference between the d_{3j}^{*} values related to η = 0 (2–2-type composite) and η = 0.01 at m_p = const does not exceed 1%. The data in figure 7 also shows that the presence of a poled porous FC matrix promotes larger $|d_{3j}^{*}|$ values at m_p = const, compared to the unpoled case, and this is due to the stronger electromechanical coupling in the composite structure (see figure 4) where an interaction between the poled FC rods becomes stronger in the presence a poled matrix surrounding the rods.

A typical example of the FC composite with the microgeometric parameters used in our calculations is shown in figure 8. Our results obtained for the composites with the poled and non-poled porous matrices for rods with a variety of aspect ratios η suggest that the main effort to improve piezoelectric performance of these porous materials is related to the formation of a highly anisotropic porous matrix at $\mu_p \geq 0.5$, with a specific microgeometry of pores (see figure 8).

A comparison of the present results on the anisotropy of d_{3j}^* [see curve 5 in figure 2(e)] to experimental data [18] on the freeze-cast PZT FC / epoxy composite shows that our parallel-connected freeze-cast porous material is characterised by a larger degree of anisotropy of d_{3j}^*, and a difference in the d_{33}^*/d_{31}^* values reaches about 20–30%. On replacing the full set of electromechanical constants of the PCR-7M FC with the full set related to the PZT-5 FC (see table 1) leads to minor changes of the studied normalised parameters and anisotropy factors of the composite shown in figure 4. These changes do not exceed 5% for the same set of m, η, μ_p, and ρ_p, and in the present paper we do not show graphs built for the similar PZT-5-based composite.

It should be added that a previously reported three-component 2–2-type composite based on the PZT-5 FC [27] exhibits a piezoelectric sensitivity that is comparable to that of the studied freeze-cast composite. The composite from work [27] consists of monolithic FC (piezoelectric) layers and cement/epoxy resin (piezo-passive) layers that are parallel-connected. In contrast to the freeze-cast composite studied in the present work, porosity of the composite [27] can be associated with the epoxy-resin inclusions in the cement medium. The $g_{33}^* / g_{33}^{(FC)}$ ratio evaluated for various samples of the composite [27] is varied from 1.4 to 2.8, and these values do not differ significantly from the $g_{33}^* / g_{33}^{(FC)}$ values on curve 3 in figure 2(e). The largest $(Q_{33}^*)^2 / (Q_{33}^{(FC)})^2$ ratio related to the composite samples [27] approaches 1.5, and this is from the range shown by curve 4 in figure 2(e).

Conclusion

In the present paper, the piezoelectric performance of PZT-type porous FC materials with varying microstructure have been analysed. Freeze casting and BURPS methods were utilised to prepare the aligned and randomly distributed pore structures. A new model, outlined in figure 4, has been proposed to link the microgeometry and effective electromechanical properties of novel porous composite materials. In this model the porous FC matrix plays the key role in forming the piezoelectric coefficients d_{3j}^* and g_{3j}^* and anisotropy of d_{3j}^* in the wide porosity range (m_p = 0.2–0.6). The effective electromechanical properties and related parameters of the composite are evaluated as functions of the volume fraction of the FC rods m, aspect ratio of the rod base η, volume fraction of air pores in the FC medium, μ_p, and aspect ratio of the air pore ρ_p. Typical values of the microgeometric parameters of the monolithic FC rod and porous FC matrix are shown in figure 8. In the present study, we have first considered variations of two aspect ratios, namely, η and ρ_p. In our calculations, we have used the full set of electromechanical constants of related PZT-type FCs to find the normalised X^* / $X^{(FC)}$ and piezoelectric anisotropy factors ζ_{d1}^* and ζ_{d2}^* of the composite. Graphs in figures 5 and 6 show that agreement between the calculated and experimental results is achieved for the parallel-connected freeze-cast porous material in the studied porosity (m_p) range.

The microgeometry (figure 4) and the presence of the transversely isotropic FC component enable us to conclude that no drastic changes in the piezoelectric

performance are observed in the aspect ratio $0 < \eta < 1$, see figure 7. The studied parallel-connected freeze-cast porous material is characterised by the relatively large piezoelectric coefficients $d_{33}^* \sim 10^2$ pC N^{-1} and $g_{33}^* \approx 40$–100 mV m N^{-1} at $d_{33}^* / |d_{31}^*| \approx 3$–$5$ and, therefore, has advantages over the conventional PZT-type FCs (see, for instance, work [3, 11, 25] and footnote in table 1). The advantages include larger piezoelectric sensitivity as well as piezoelectric anisotropy which are the important design parameters for transducer, sensor and energy-harvesting applications.

Acknowledgements

The authors would like to thank Prof. Dr A A Nesterov and Prof. Dr A E Panich (Southern Federal University, Russia) for their research interest in the piezoelectric performance of modern composites and related materials. Prof. Dr C R Bowen acknowledges funding from the European Research Council under the European Union's Seventh Framework Programme (FP/2007-2013) / ERC Grant Agreement no. 320963 on Novel Energy Materials, Engineering Science and Integrated Systems (NEMESIS). In the present paper, the results on the research project No. 11.1627.2017/PCh have been represented within the framework of the state task in the scientific activity area at the Southern Federal University, and Prof. Dr V Yu Topolov acknowledges relevant funding. This research has been performed using the equipment of the Centre of Collective Use ‘High Technologies’ at the Southern Federal University.

References

[1] Wersing W, Lubitz K and Mohaupt J 1986 Dielectric, elastic and piezoelectric properties of porous PZT ceramics *Ferroelectrics* **68** 77–97

[2] Dunn M 1995 Effects of grain shape anisotropy, porosity, and microcracks on the elastic and dielectric constants of polycrystalline piezoelectric ceramics *J. Appl. Phys.* **78** 1533–41

[3] Topolov VYu and Bowen CR 2009 *Electromechanical properties in composites based on ferroelectrics* (London: Springer)

[4] Lopatin SS and Lupeiko TG 1991 Properties of the porous piezoelectric ceramic of the lead zirconate-titanate type *Neorganicheskie Materialy* **27** 1948–51 (in Russian)

[5] Bowen CR, Perry A, Lewis ACF and Kara H 2004 Processing and properties of porous piezoelectric materials with high hydrostatic figures of merit *J. Europ. Cer. Soc.* **24** 541–5

[6] Praveen Kumar B, Kumar HH and Kharat DK 2005 Study on pore-forming agents in processing of porous piezoceramics *J. Mater. Sci.: Mater. Electron.* **16** 681–6

[7] Filippov SE, Vorontsov AA, Brill OE and Topolov VYu 2014 Microgeometry, piezoelectric sensitivity and anisotropy of properties in porous materials based on Pb(Zr, Ti)O_3 *Funct. Mater. Lett.* **7** 1450029–6 p

[8] Lewis RWC, Dent ACE, Stevens R and Bowen CR 2011 Microstructural

modelling of the polarization and properties of porous ferroelectrics *Smart Mater. Struct.* **20** 085002–6 p

[9] Zhang Y, Roscow J, Lewis R, Khanbareh H, Topolov VYu, Xie M and Bowen CR 2018 Understanding the effect of porosity on the polarisation-field response of ferroelectric materials *Acta Mater*. **154** 100–12

[10] Newnham RE 2005 *Properties of materials. Anisotropy, symmetry, structure* (New York: Oxford University Press)

[11] Xu Y 1991 *Ferroelectric materials and their applications* (Amsterdam, London, New York, Toronto: North-Holland)

[12] Guo R, Wang C-A, Yang A and Fu J 2010 Enhanced piezoelectric property of porous lead zirconate titanate ceramics with one dimensional ordered pore structure *J. Appl. Phys.* **108** 124112–4 p.

[13] Xu TT and Wang C-A 2015 Grain orientation and domain configuration in 3-1 type porous PZT ceramics with ultrahigh piezoelectric properties *J. Am. Ceram. Soc.* **98** 2700–02

[14] Xu TT and Wang C-A 2016 Control of pore size and wall thickness of 3-1 type porous PZT ceramics during freeze-casting process *Mater. Design* **91** 242–7

[15] Zhang Y, Xie M, Roscow J, Bao Y, Zhou K, Zhang D and Bowen CR 2017 Enhanced pyroelectric and piezoelectric properties of PZT with aligned porosity for energy harvesting applications *J. Mater. Chem. A* **5** 6569–80

[16] Zhang Y, Roscow J, Xie M and Bowen C 2018 High piezoelectric sensitivity

and hydrostatic figures of merit in unidirectional porous ferroelectric ceramics fabricated by freeze casting *J. Europ. Cer. Soc*. **38** 4203–11

[17] Newnham RE, Skinner DP and Cross LE 1978 Connectivity and piezoelectric-pyroelectric composites *Mater. Res. Bull*. **13** 525–36

[18] Xu T and Wang C-A 2014 Piezoelectric properties of a pioneering 3-1 type PZT/epoxy composites based on freeze-casting processing *J. Am. Cer. Soc*. **97** 1511–6

[19] *European Standard* EN 623-2:1993 Advanced technical ceramics – Monolithic ceramics – General and textural properties – Part 2 – Determination of density and porosity

[20] Hong C, Zhang X, Han J, Du J and Zhang W 2010 *Mater. Chem. Phys*. **119** 359–62

[21] Moulson AJ Herbert JM 2003 *Electroceramics: materials, properties, application* (Chicester: John Wiley & Sons Ltd,)

[22] Hooker MW 1998 Properties of PZT-based piezoelectric ceramics between – 150 and 250 °C. In *NASA contractor report. National Aeronautics and Space Administration, Langley Research Center*, 208708

[23] Huang JH and Yu S 1994 Electroelastic Eshelby tensors for an ellipsoidal piezoelectric inclusion *Compos. Engin*. **4** 1169–82

[24] Ikeda T 1990 *Fundamentals of piezoelectricity* (Oxford, New York, Toronto: Oxford University Press)

[25] Berlincourt DA, Cerran DR and Jaffe H 1964 Piezoelectric and piezomagnetic

materials and their function in transducers. In: Mason W (ed.) *Physical acoustics. Principles and methods. Vol. 1. Methods and devices. Pt A* (New York, London: Academic Press) 169–270

[26] Roscow JI, Zhang Y, Kraśny MJ, Lewis RWC, Taylor J and Bowen CR 2018 Freeze cast porous barium titanate for enhanced piezoelectric energy harvesting *J. Phys. D: Appl. Phys*. 51 225301–18 p

[27] Dongyu X, Xin C, Banerjee S, Lei W and Shifeng H 2015 Dielectric, piezoelectric and damping properties of novel 2-2 piezoelectric composites *Smart Mater. Struct*. **24** 025003–8 p

Table 1. Experimental room-temperature values of elastic moduli c_{ab}^{E} (in 10^{10} Pa), piezoelectric coefficients e_{ij} (in C m^{-2}) and dielectric permittivities ε_{pp}^{ξ} of poled FCs

	PZT-5[a] [25]	PCR-7M[b] [3]
c_{11}^{E}	12.1	13.3
c_{12}^{E}	7.54	9.2
c_{13}^{E}	7.52	9.1
c_{33}^{E}	11.1	12.5
c_{44}^{E}	2.11	2.28
e_{31}	–5.4	–9.5
e_{33}	15.8	31.1
e_{15}	12.3	12.3
$\varepsilon_{11}^{\xi}/\varepsilon_0$	916	540
$\varepsilon_{33}^{\xi}/\varepsilon_0$	830	830

[a] For poled PZT-5 FC, d_{33} = 373 pC N^{-1}, d_{31} = –170 pC N^{-1}, g_{33} = 24.2 mV m N^{-1}

[b] For poled PCR-7M FC, d_{33} = 755 pC N^{-1}, d_{31} = –347 pC N^{-1}, g_{33} = 17.2 mV m N^{-1}

Figure captions to the paper SMS-108293 "Piezoelectric performance of PZT-based materials with aligned porosity: experiment and modeling" by Y Zhang et al.

Figure 1. Schematic of freeze-cast PZT with parallel-connection and series-connection directions.

Figure 2. Micrographs of the parallel-connected freeze-cast composite (a)–(d) and room-temperature dependences of its normalised parameters X^* / $X^{(FC)}$ and piezoelectric anisotropy factor d_{33}^*/d_{31}^* on porosity m_p (e). In micrographs (a)–(c), the poling direction is vertical. In micrograph (d), orientations of some FC-walls are shown with dash lines. Graph (e) has been built by using experimental values of the piezoelectric coefficients d_{3j}^* and dielectric permittivity $\varepsilon_{33}^{*\sigma}$ at mechanical stress σ = const.

Figure 3. Micrographs of the composite with randomly distributed pores (a and b) and room-temperature dependences of its normalised parameters X^* / $X^{(FC)}$ and piezoelectric anisotropy factor d_{33}^*/d_{31}^* on porosity m_p (c and d). In micrographs (a) and (b), the poling direction is vertical. Graphs (c) and (d) have been built using experimental values of the piezoelectric coefficients d_{3j}^* and dielectric permittivity $\varepsilon_{33}^{*\sigma}$ at mechanical stress σ = const.

Figure 4. Schematic of the studied composite (a) and sections of the composite sample by the (X_2OX_3) plane (b) and by the (X_1OX_2) plane (c) of the rectangular co-ordinate system ($X_1X_2X_3$). m is the volume fraction of monolithic FC rods, and 1 – m is the volume fraction of the porous FC matrix. In inset of figure (a) μ_p is the volume fraction of air pores in the porous FC matrix, 1 – μ_p is the volume fraction of FC in the porous matrix, and a_{p1} and a_{p3} are semi-axes of the air pore therein. In figure (c) a_1 and a_2 are semi-axes of the elliptical cross section of the FC rod.

Figure 5. Calculated dependences of normalised piezoelectric coefficients d_{31}^{*} / $d_{31}^{(FC)}$ (a), d_{32}^{*} / $d_{31}^{(FC)}$ (b), d_{33}^{*} / $d_{33}^{(FC)}$ (c), and g_{33}^{*} / $g_{33}^{(FC)}$ (d), normalised energy harvesting figure of merit $(Q_{33}^{*})^2/(Q_{33}^{(FC)})^2$ (e), and piezoelectric anisotropy factors ζ_{d1}^{*} (f) and ζ_{d2}^{*} (g) on porosity m_p of the 1–3–0 composite (see the schematic in figure 4) with the non-poled porous FC matrix. Calculations have been performed by using the full set of electromechanical constants of the PCR-7M FC from monograph [3], see data in table 1. Experimental curves are related to the parallel-connected freeze-cast porous PZT-based composite at room temperature.

Figure 6. Dependences of normalised piezoelectric coefficients d_{31}^{*} / $d_{31}^{(FC)}$ (a), d_{32}^{*} / $d_{31}^{(FC)}$ (b), d_{33}^{*} / $d_{33}^{(FC)}$ (c), and g_{33}^{*} / $g_{33}^{(FC)}$ (d) on porosity m_p of the 1–3–0 composite (see the schematic in figure 4) with the poled porous FC matrix. Experimental curves are related to the parallel-connected freeze-cast porous PZT-based composite at room temperature.

Figure 7. Dependences of normalised piezoelectric coefficients d_{3j}^{*} / $d_{3j}^{(FC)}$ of the 1–3–0 composite (see the schematic in figure 4) on the aspect ratio of the FC rod base $0.01 \le \eta \le 0.90$ at porosity $m_p = 0.20$ (a), 0.30 (b) and 0.60 (c). The aspect ratio of the air pore is $\rho_p = 10$.

Figure 8. Schematic of the 1–3–0 composite at typical values of volume fractions of air pores in the matrix μ_p and aspect ratios of the rods η and pores ρ_p (see legends in graphs of figures 5 and 6). Porosity of the composite $m_p = (1-m)\mu_p$ is varied by changing m and μ_p.

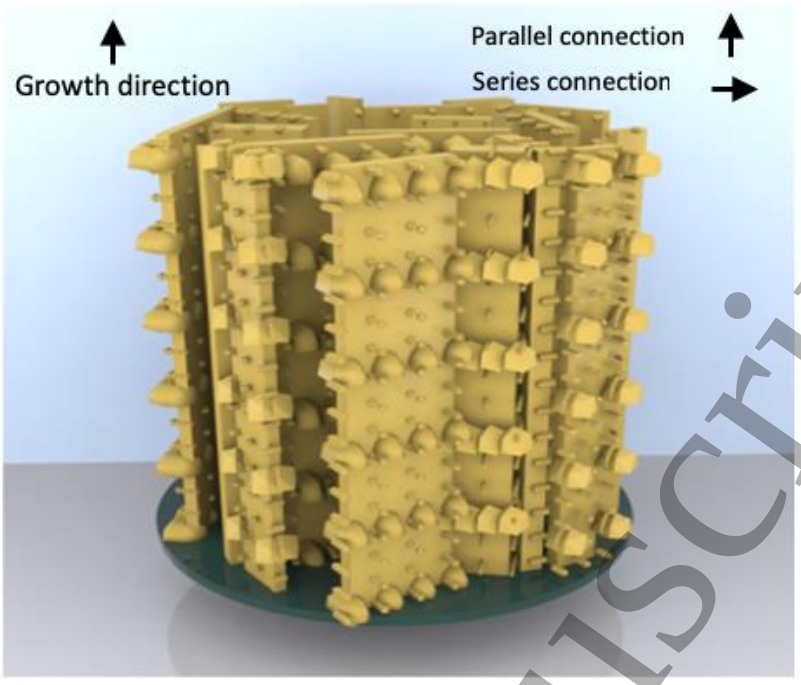

Fig. 1

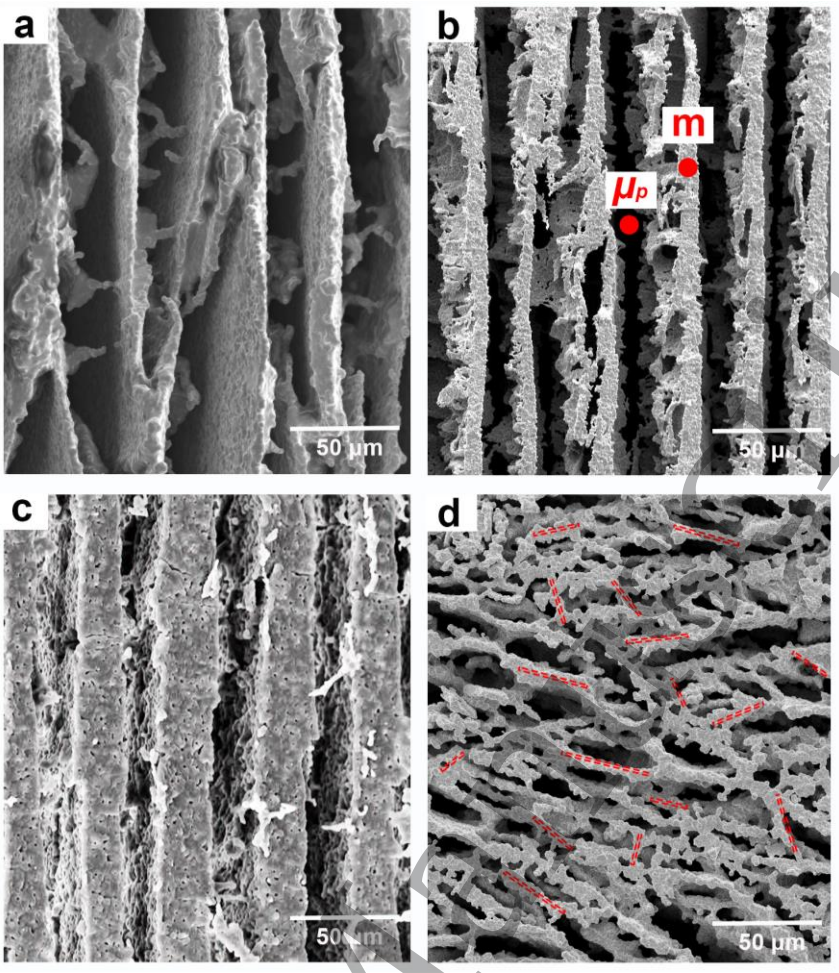

a–d

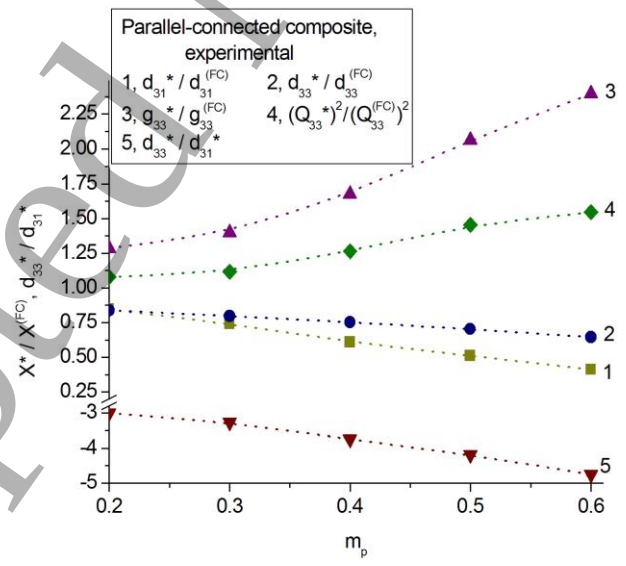

e

Fig. 2

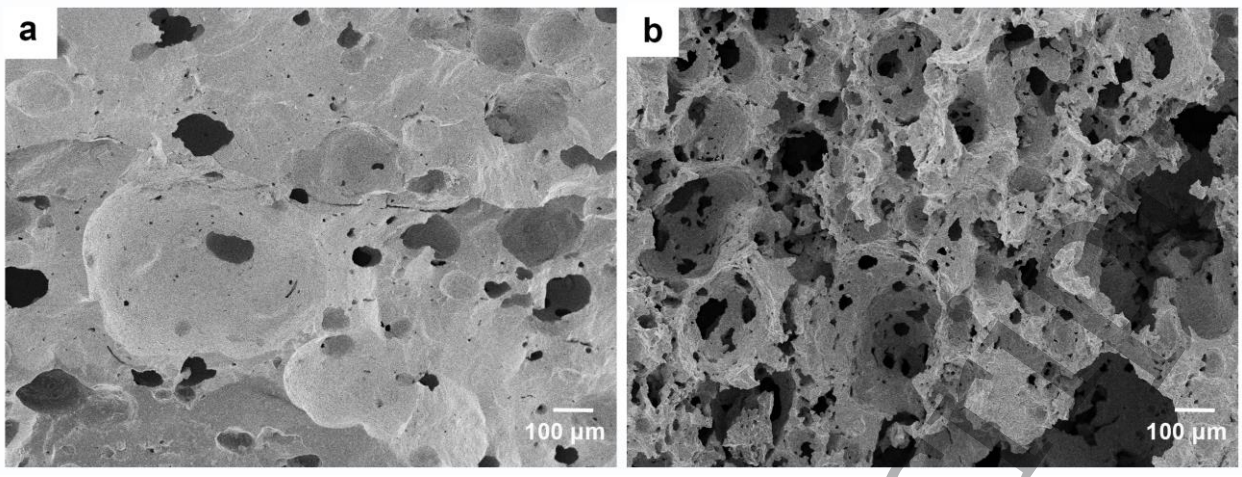

a b

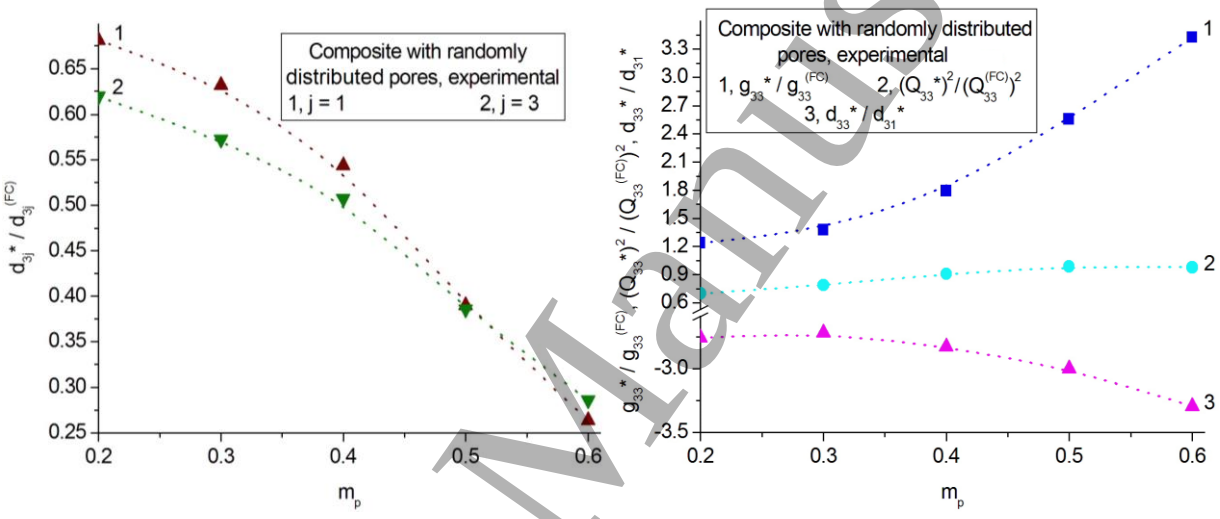

c d

Fig. 3

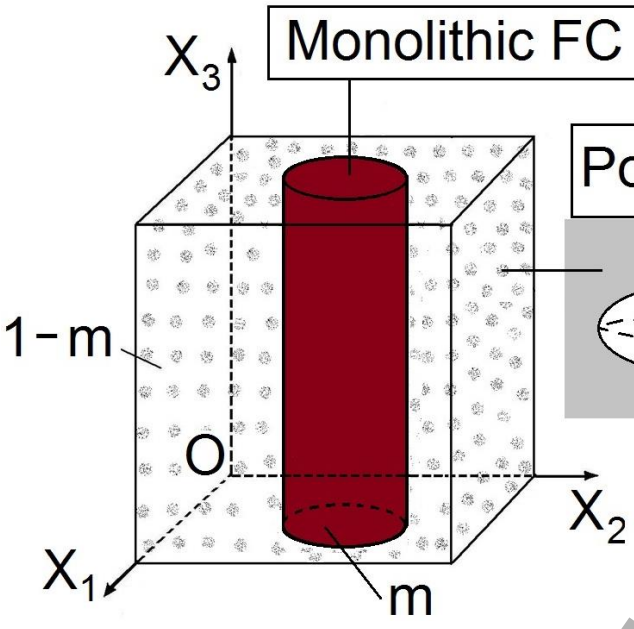

a

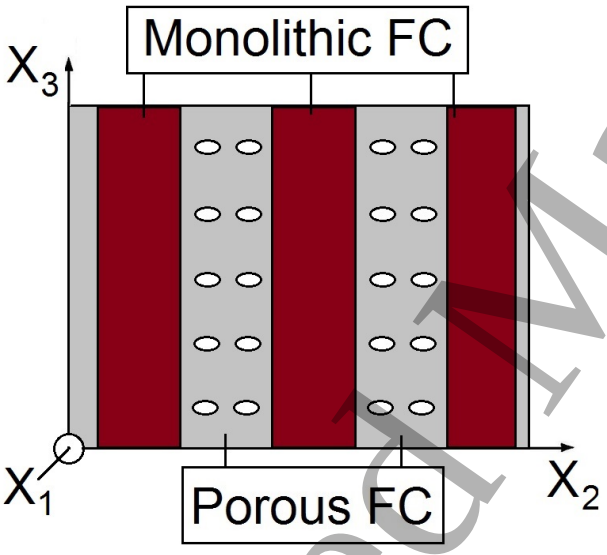

b

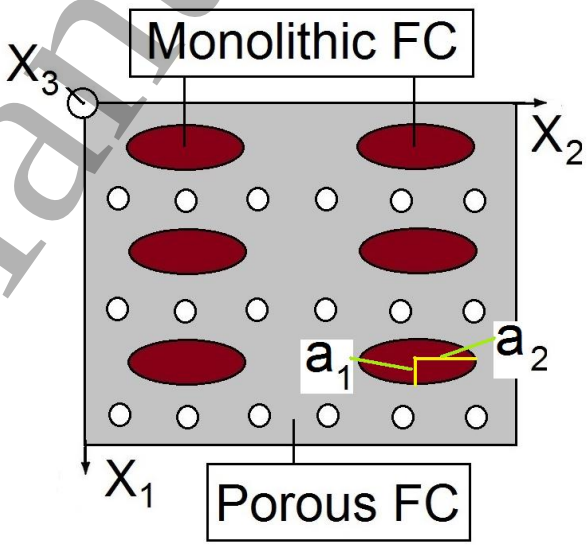

c

Fig. 4

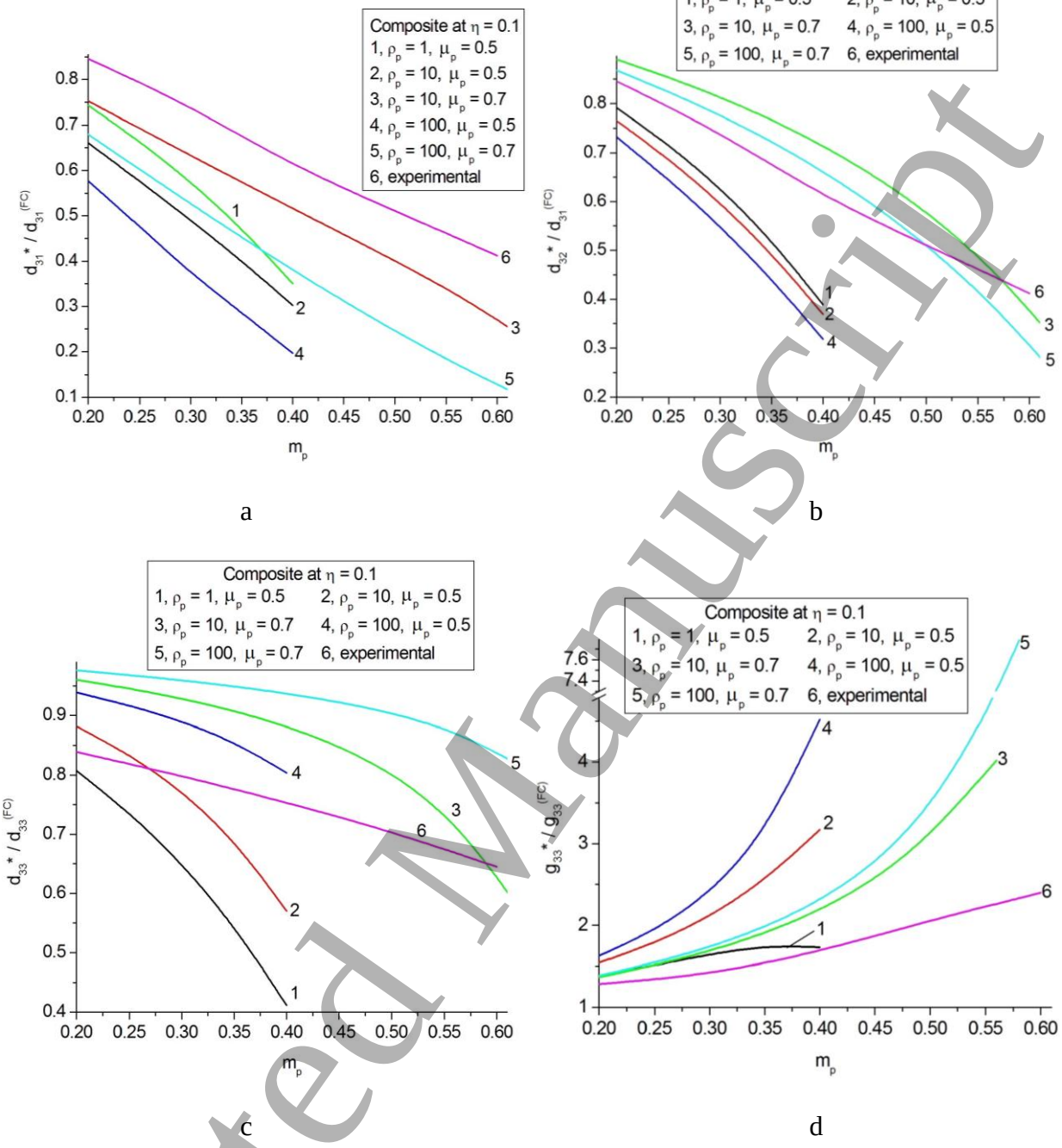

Fig. 5 (*continued*)

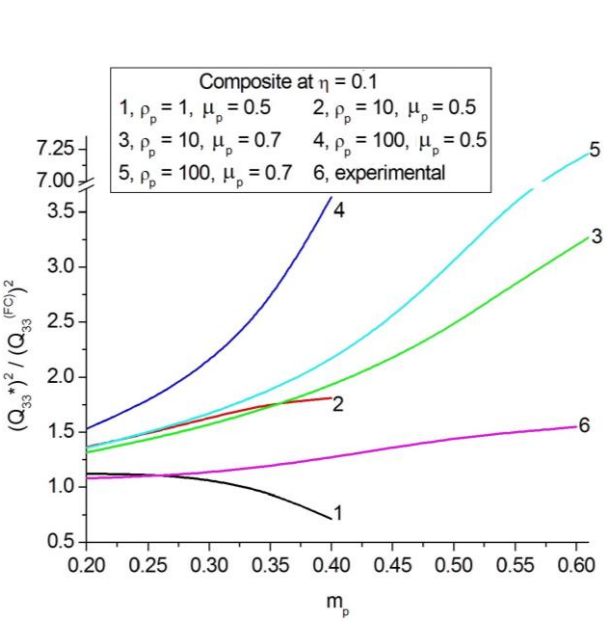

e

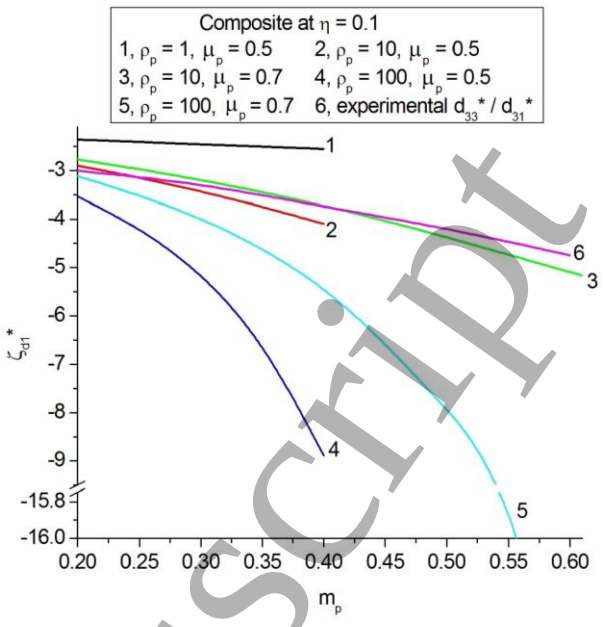

f

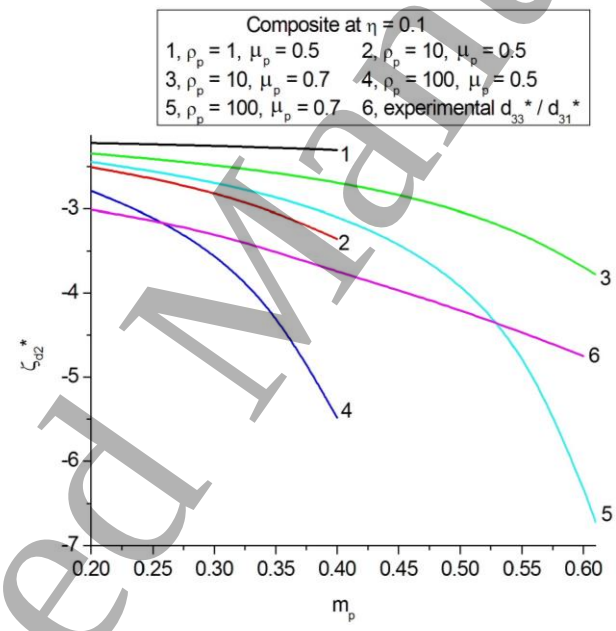

g

Fig. 5

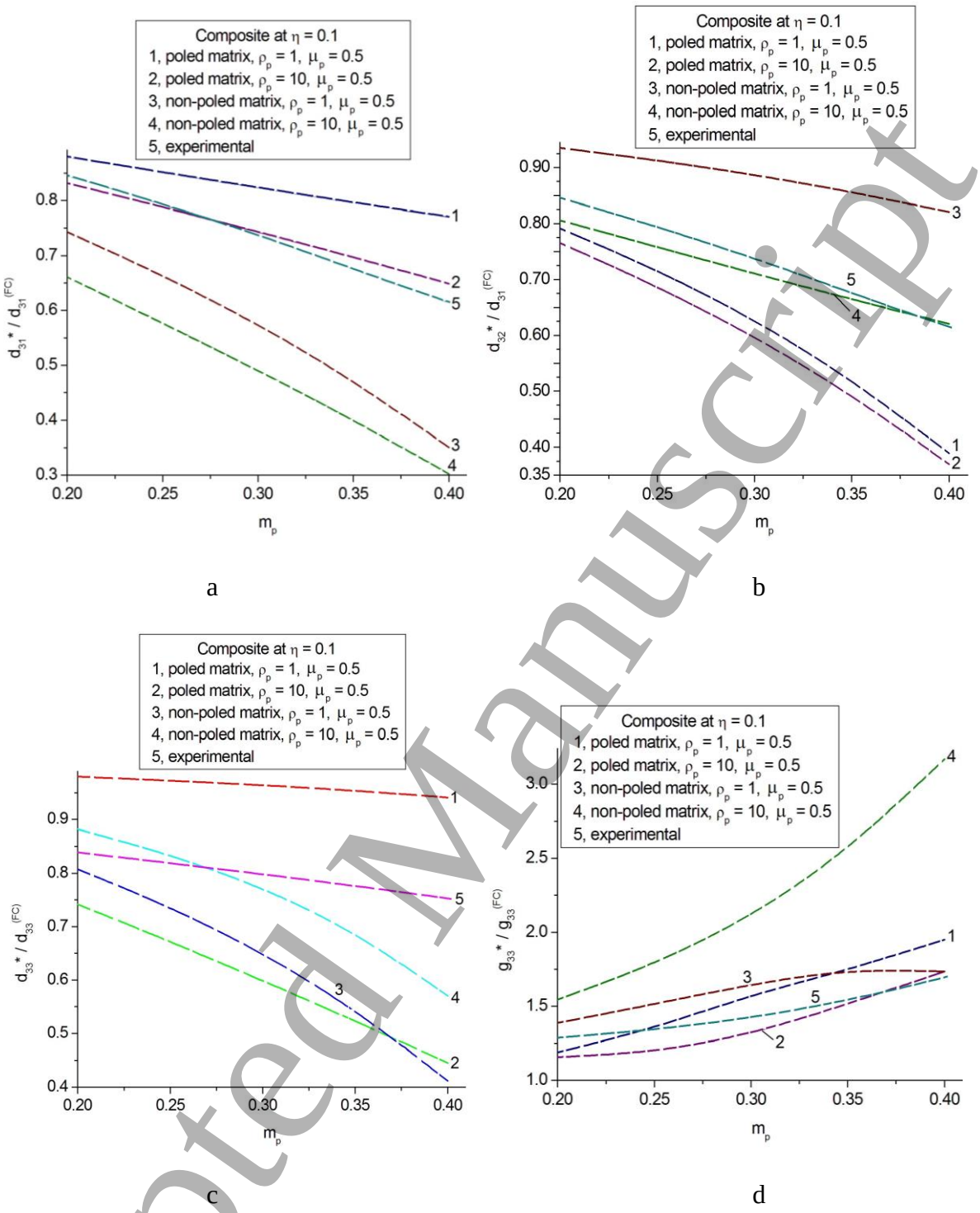

Fig. 6

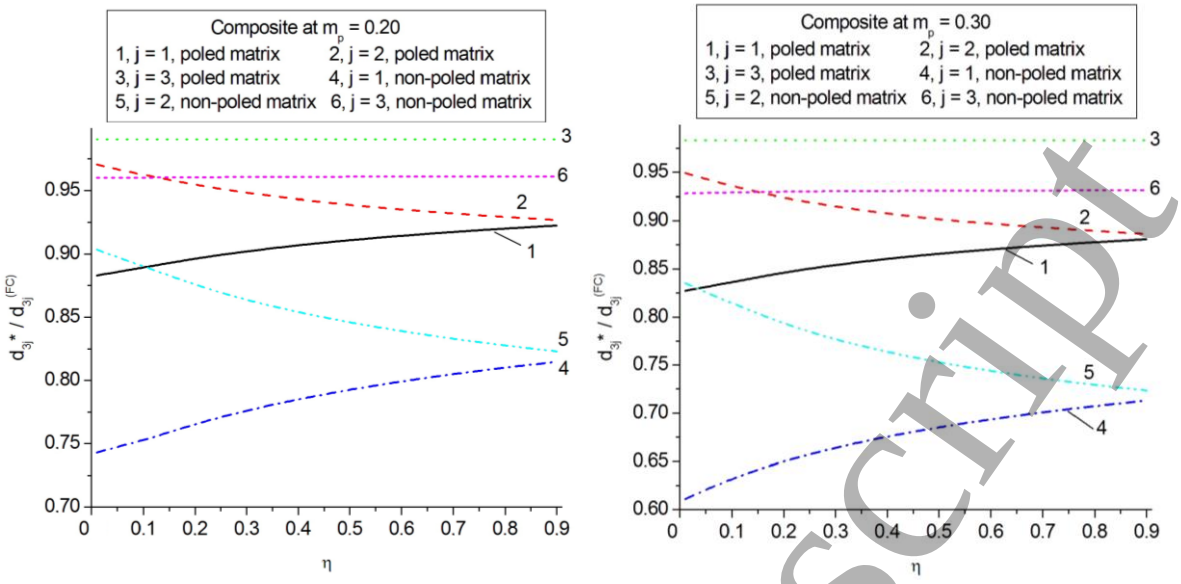

a b

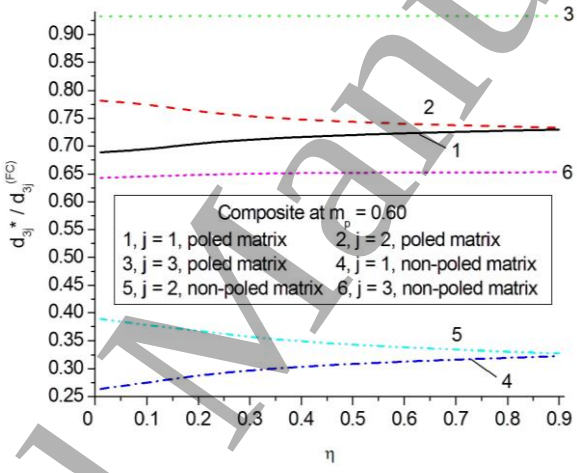

c

Fig. 7

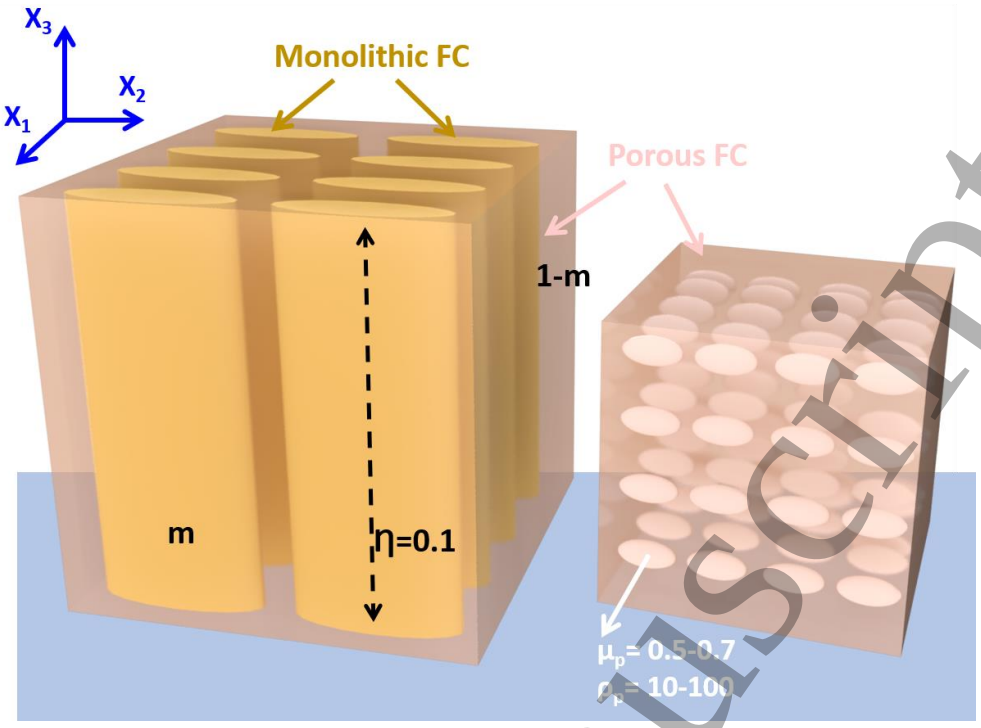

Fig. 8